Journal of Materials Chemistry A

PAPER

View Article Online
View Journal | View Issue

Cite this: J. Mater. Chem. A, 2017, 5, 8408

Cu-doped P2-$Na_{0.5}Ni_{0.33}Mn_{0.67}O_2$ encapsulated with MgO as a novel high voltage cathode with enhanced Na-storage properties†

Hari Vignesh Ramasamy,[a] Karthikeyan Kaliyappan,[bc] Ranjith Thangavel,[a] Vanchiappan Aravindan,[d] Kisuk Kang,[e] Dae Ung Kim,[a] Yongll Park,[a] Xueliang Sun[b] and Yun-Sung Lee*[a]

Received 1st December 2016
Accepted 4th April 2017

DOI: 10.1039/c6ta10334k

rsc.li/materials-a

We report a novel P2-type $Na_{0.5}Ni_{0.26}Cu_{0.07}Mn_{0.67}O_2$ (NCM) mixed oxide obtained by conventional solid-state method as a prospective cathode for sodium-ion battery (SIB) applications. X-ray diffraction analysis shows that NCM exhibits a hexagonal structure with a $P6_3/mmc$ (No. 194) space group, in which Na-ions are located in a prismatic environment. The introduction of Cu into the lattice enhances its structural stability, showing a capacity retention of 83% after 100 cycles, which is much better than its native compound. MgO encapsulation was performed to further improve the interfacial kinetics and suppress P2–O2 phase transition. MgO coating significantly improves the electrochemical activity at high cut-off voltages, for instance, highest capacity of 131 mA h g^{-1} was noted with superior rate performance of 83 and 51 mA h g^{-1} at 5 and 20C, respectively. As expected, dual modification by Cu-ion doping and MgO coating provides a novel strategy for designing high-rate SIB cathodes.

1. Introduction

Over the past decades, Li-ion batteries (LIBs) have been predominantly used to power most of the portable electronic devices, (hybrid) electric vehicles, aerospace applications, and grids due to their high energy density, flexibility, and long cycle lifetimes.[1] However, high cost, scarcity of Li-deposits in the earth's crust (0.006 wt%) and safety concerns for operation under extreme environmental conditions constrain their applications. Sodium-ion battery (SIB) is considered as better alternative to LIB due to the similar storage mechanism.[2] Owing to the natural abundance (fourth most abundant element on earth) along with its wide distribution (*e.g.*, sea salt and rock salt) and low cost of sodium, SIBs can be considered promising candidates for large-scale energy storage systems, where cost aspect is of prime importance and decent gravimetric energy density is sufficient.[3,4] However, finding a suitable cathode that is capable of withstanding high stress caused by the larger Na-ion is highly challenging. Various cathode materials such as layered oxides,[5] polyanionic compounds,[6] redox-active polymers,[7] and Prussian blue analogues[8] have been found to host Na ions in their crystal structure. Among them, layered transition metal oxides exhibit various advantages like simple structure, good electrochemical performance, and ease of synthesis.[9] Based on alkali ion occupancies, these layered oxides can be classified as prismatic (P2) or octahedral (O3), where the numeral indicates the number of transition metal layers in the repeating unit cell.[10] Among metal oxides, compounds of $NaMO_2$ (M = Co, Ni, Mn, Fe, *etc.*) have been intensively investigated due to their unique electrochemical properties.[11–14] Ternary and quaternary systems utilizing the synergistic effect of various transition metal oxides such as $Na_{0.67}Ni_{0.15}Co_{0.2}Mn_{0.65}O_2$,[15] $Na_{0.67}Ni_{0.15}Fe_{0.2}Mn_{0.65}O_2$ (ref. 5) and $NaNi_{1/4}Co_{1/4}Fe_{1/4}Mn_{1/8}Ti_{1/8}O_2$ (ref. 16) have also been studied. Furthermore, P2-type Na–Ni–Mn–O materials are considered to be suitable SIB cathode materials due to their stability in air, low cost, ease of synthesis, and high theoretical capacity of above 250 mA h g^{-1}.[17] Lu *et al.*[18] reported P2-type $Na_{2/3}Ni_{1/3}Mn_{2/3}O_2$ as a cathode with complete extraction/re-insertion of Na-ions in its structure. Moreover, high theoretical capacity of 173 mA h g^{-1} was noted, but severe capacity fading due to P2–O2 phase transition above 4.2 V was a major setback. Limiting cut-off voltage appeared to be a good option, but it certainly decreased the reversible capacity and energy density. Moreover, complete removal of Na ions in a wider operating window led to increased repulsion of oxygen atoms in adjacent layers.[19] Considering this problem, cationic substitution

[a]Faculty of Applied Chemical Engineering, Chonnam National University, Gwang-ju 500-757, Republic of Korea. E-mail: leeys@chonnam.ac.kr

[b]Department of Mechanical and Materials Engineering, University of Western Ontario, London N6A 5B9, Canada

[c]Department of Chemical Engineering, University of Waterloo, Waterloo, Ontario N2L 3G1, Canada

[d]Energy Research Institute@NTU (ERI@N), Nanyang Technological University, Singapore 637553. E-mail: aravind_van@yahoo.com

[e]Department of Material Science and Engineering, Seoul National University, 599 Gwanangno, Gwanak-gu, Seoul 151-742, South Korea

† Electronic supplementary information (ESI) available. See DOI: 10.1039/c6ta10334k

could be an effective strategy to improve the structural stability of this material. Several researchers substituted Mg, Al, Fe, Co, Ti, Zn, and Li in the P2 Na–Ni–Mn–O structure, which eventually led to (i) an increase in structural stability, thereby resulting in a smooth and enhanced voltage plateau,[20,21] (ii) suppression of the Na^+/vacancy ordering,[17] (iii) prevention of cation mixing in Na sites,[22] and (iv) suppression of Jahn–Teller distortion of Mn ions.[23] Copper, being a robust and cheap element, has been used as an efficient doping material in Li-ion battery cathodes, for example Cu-doped $LiCoO_2$ is highly stable at elevated voltages. Similarly, spinel $LiCu_{0.12}Ni_{0.38}Mn_{1.5}O_4$ exhibited increased capacity retention due to reduced cation ordering, and $LiCu_{0.25}Ni_{0.25}Mn_{1.5}O_4$ has shown low Li-ion diffusion barrier with good rate capability.[24–26] Thus far, few Cu-based cathode materials have been reported for SIBs.[27–30] Extending the study in this line, we investigated the electrochemical properties of Cu-substituted mixed oxides with higher operating window. At these voltages, durability of SIB was mainly affected by side reactions that occurred at the electrode/electrolyte interface.[31] Hence, it was essential to design a suitable strategy to minimize these drawbacks and improve the interfacial reactions in order to obtain high-rate cathodes with good durability. Surface modification with carbon/metal oxides yielded good results for LIB by preventing the unwanted side reaction with electrolytic solutions.[32–36] However, only few reports are available on metal oxide coatings for SIB cathode; for instance, Karthikeyan *et al.*[31] used atomic layer deposition to coat Al_2O_3 and studied the impact of Al_2O_3 layer thickness on the electrochemical performance of $Na_{0.66}Mn_{0.54}Ni_{0.13}Co_{0.13}O_2$ at high voltages.

Herein, we studied the electrochemical performance of Cu-substituted mixed oxides in a high-voltage range of 2–4.5 V. Thus far, the application of MgO coating to SIB materials has not been reported. Hence, this study presents a novel strategy for designing high-rate SIB cathode materials. Based on the results obtained from electrochemical studies, we further modified the surface with MgO coating by solution-free melt impregnation to mitigate the degradation of layered oxide. MgO has been used as a coating material due to its ability to mitigate the volume change occurring during Li-ion insertion/extraction in LIB.[37] In addition to preventing cathodic side reactions, MgO coating drastically reduces the interfacial resistance during high-potential cycling, as confirmed by electrochemical impedance spectroscopy (EIS) studies. Extensive powder and electrochemical studies have been performed and described in detail.

2. Experimental

2.1. Synthesis of $Na_{0.5}Ni_{0.33}Mn_{0.67}O_2$ (NM) and $Na_{0.5}Ni_{0.26}Cu_{0.07}Mn_{0.67}O_2$ (NCM)

The P2-type $Na_{0.5}Ni_{0.33}Mn_{0.67}O_2$ (NM) was synthesized using a conventional solid-state method. Stoichiometric amounts of Na_2CO_3 (Sigma Aldrich, 98%), nickel(II) acetate tetrahydrate (Sigma Aldrich, 99%), and manganese(II) oxide (Sigma Aldrich, >98%) were ground for 0.5 h using a mortar and pestle. The resultant powder was pressed into pellets, heated to 900 °C for 15 h at a heating rate of 5 °C min^{-1} in a muffle furnace, and slowly cooled to room temperature to yield NM. The same procedure was repeated to obtain NCM under similar conditions, while copper(II) oxide was used as a source of Cu (Scheme 1(a)).

2.2. Synthesis of $Na_{0.5}Ni_{0.26}Cu_{0.07}Mn_{0.67}O_2$/MgO (NCM/MgO)

Coating of NCM by MgO was performed by melt impregnation method wherein, magnesium nitrate was mixed with 1 g of the synthesized material using a mortar and pestle (Scheme 1(b)). The mixed powders were made into pellets and subjected to two-step calcination process: first maintained at 120 °C for 2 h, followed by calcination at 500 °C for 2 h. The resulting sample was named as NCM/MgO.

2.3. Material characterization

Crystal structures were characterized by X-ray diffraction (XRD; Cu K_α radiation, Rint 1000, Rigaku, Japan) in 2θ range of 5–90°. Lattice parameters were determined by Rietveld refinement using GSAS software. The particle morphology, elemental composition and internal structure were evaluated using Field-emission scanning electron microscopy (FE-SEM, S-4700, Hitachi, Japan) coupled with an energy-dispersive X-ray spectroscopy (EDX) module, and high-resolution transmission electron microscopy (HR-TEM; JEM-2000, EX-II, JEOL, Japan). The stoichiometry was determined with inductively coupled plasma atomic emission spectroscopy (ICP-AES analysis, Perkin Elmer, OPTIMA 8300, USA). XPS measurements (Multilab 2000, UK) were performed to determine the chemical oxidation sates of Mn, Ni, and Co on the compound surface. FTIR measurements were performed using an IR Prestige-21 spectrometer (Shimadzu corp., Japan) to identify local structural changes caused by inactive cationic substitution.

2.4. Electrochemical measurements

The electrochemical studies of all samples were performed using CR2032 coin cells assembled inside a glovebox under a controlled atmosphere of ultrapure argon. The cells consisted

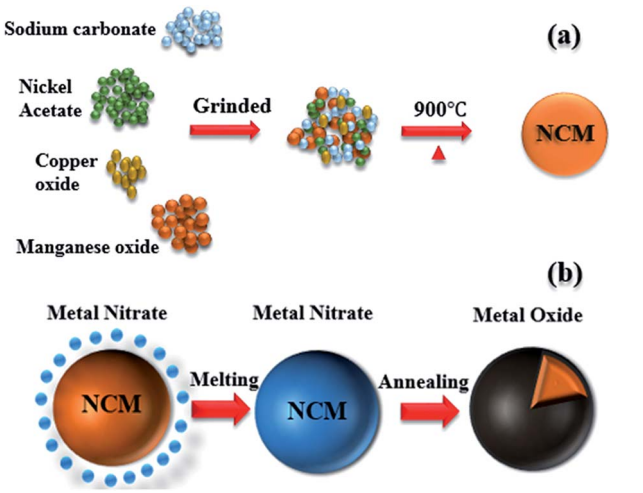

Scheme 1 Schematic showing (a) NCM synthesis and (b) MgO coating by melt impregnation.

of the synthesized material as the cathode and metallic Na as the anode separated by a polypropylene separator, with 1 M $NaClO_4$ in a mixture of ethylene carbonate (EC) and diethyl carbonate (DEC) (1 : 1, v/v) as the electrolyte. The cathode materials were prepared by mixing 2.5 mg of active material with 0.5 mg of Ketjen black and 0.5 mg of teflonized acetylene black (TAB-2). The obtained mixtures were pressed on stainless steel current collector and dried in an oven at 160 °C for 4 h before cell fabrication. Charge–discharge (C–DC) studies were performed for different voltage ranges at current rates varying from 0.25 to 20C using an Arbin BT-2000 battery test system. Cyclic voltammetry and EIS analyses were conducted using an electrochemical analyzer (SP-150, Biologic, France).

3. Results and discussion

The XRD peaks of pristine and Cu-doped and MgO-coated materials reveal a P2-type layered structure with a $P6_3/mmc$ (no. 194) space group (Fig. S1†). The XRD Rietveld refinement pattern presented in Fig. 1 suggests the phase purity of all the three samples. Intense reflections correspond to highly crystalline nature of the samples prepared and indexed accordingly. Furthermore, Cu-doped samples do not exhibit any additional peaks, clearly indicating that the substitution of metal ions in transition metal layer occurs without any phase change of the parent compound. Similarly for NCM/MgO, no reflections associated with MgO were detected, thereby suggesting that MgO coating on the surface might be either ultrathin or amorphous. The NCM hexagonal crystal structure unit cell with alternating alkali and transition metal layers is given in Fig. 1d, in which it can be observed that Na ions occupy two different prismatic sites: Na (1) position that shares faces with MO_6 octahedra in the layers, and Na (2) position that shares only corresponding edges.[19] The obtained lattice and other refined parameters have been summarized in Table S1.† After Cu-doping, lattice parameter values increase due to larger ionic radius of Cu ions (1.28 Å) compared to those of Ni ions (1.24 Å). The higher c/a ratio (3.8) denotes increased crystallinity of the cathode. To analyze local environment changes of the cathode after Cu substitution, FTIR studies were conducted, and the results are given in Fig. S2.† The appearance of three intense peaks at 440, 513, and 1448 cm^{-1} could be due to asymmetric stretching modes of MO_6 octahedra, bending modes of O–M–O units,[20] and presence of carbonate functional groups on the compound surface,[38] respectively. The results of ICP-AES analysis (Table S2†) were found to be in good agreement with theoretical values. Energy-dispersive X-ray spectroscopy (Fig. S3†) was used to confirm the identity of elements present in NCM cathode surface along with MgO.

FE-SEM images (Fig. 2a–c) of all the samples show similar morphology irrespective of the small amount of Cu doped into the lattice. The high-temperature precursor calcination at 900 °C for 15 h results in large aggregated secondary particles with high crystallinity and an average crystallite size of 2–5 μm. Fig. 2d–f show the elemental distribution of Mg, Mn, and Ni observed using EDX elemental mapping. The amount of MgO on the surface was found to be 2.0 wt%. Fig. 2g and h show high resolution TEM images of NCM/MgO. The MgO surface coating with a thickness of 1.3 nm was clearly visible in the corresponding HR-TEM images. The interplanar spacings of 2.1 and 1.0 Å obtained from the lattice fringes correspond to [013] and [025] planes, respectively. Furthermore, single crystalline nature of the sample was confirmed by selected area electron diffraction (SAED) pattern, and the results are given in Fig. 2i. From Fig. S4a–c,† it can be concluded that MgO is well coated on the surface with a clear boundary between the bulk and surface

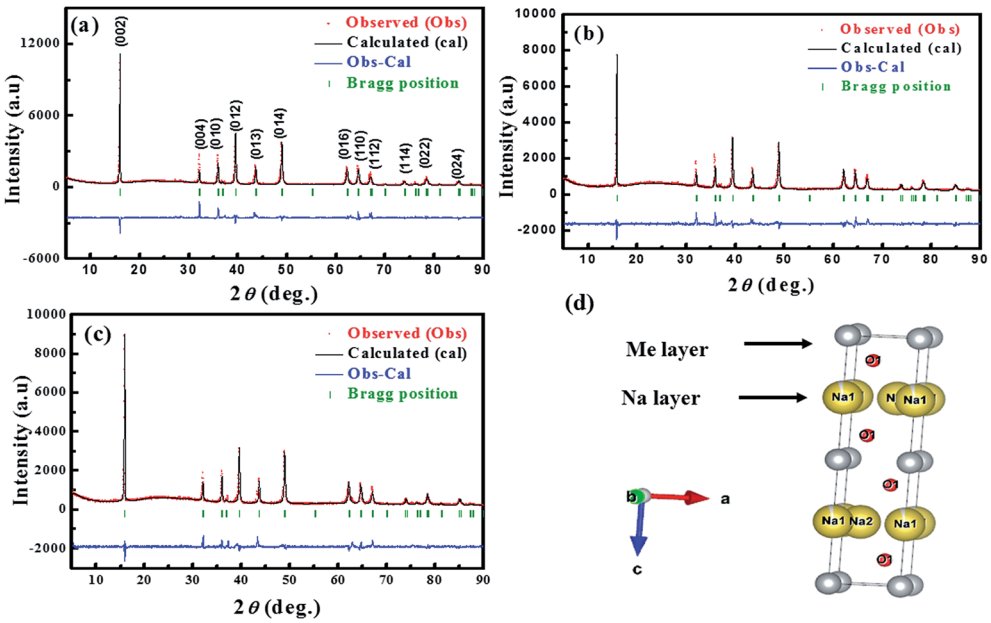

Fig. 1 Rietveld refinement of the X-ray diffraction patterns of (a) NM, (b) NCM, and (c) NCM/MgO. (d) Schematic showing the P2-type structure unit cell.

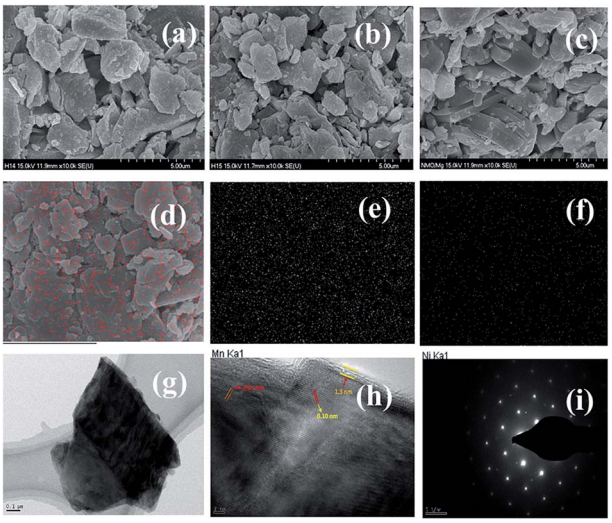

Fig. 2 SEM images of (a) NM, (b) NCM, and (c) NCM/MgO. Elemental mapping of (d) Mg, (e) Mn and (f) Ni. (g and h) HR-TEM images of MgO-coated sample, (i) SAED pattern showing high crystallinity of NCM/MgO.

coated layer. Moreover, the transport and storage path of Na ion is clearly visible from the respective images. All these results confirm the presence of single crystalline particles.

In order to understand NCM chemical composition and surface oxidation states, XPS analyses were performed, and the results are given in Fig. S5.† Fig. S5a† shows the survey spectrum of NCM. The appearance of peaks at 1070.29, 932.75, 854.11, 641.38, 530.26 and 284.6 eV confirms the presence of Na, Cu, Ni, Mn, C, and O, respectively. Fig. S5b–g† show the deconvoluted spectra of individual spin orbit. The Mn 2p peak can be deconvoluted into four different characteristic peaks: the ones appearing at binding energies of 641.38 and 653.1 eV correspond to Mn 2p3 and Mn 2p1, respectively, while those at 642.78 and 654.54 eV are satellite peaks.[17] Thus, the oxidation state of Mn was confirmed as +4. The high-temperature calcination for 15 h in air leads to partial evaporation of Na, which is responsible for the increased valence state of Mn.[39] The Ni 2p peak can be separated into four peaks, corresponding to Ni 2p1 (871.63 eV) and Ni 2p3 (854.11 eV), with other peaks (860.43 and 877.89 eV) being satellites. Herein, oxidation state of Ni is +2.[17] The two distinct peaks appearing at 953.00 and 932.74 eV correspond to Cu 2p1 and Cu 2p3, respectively. The appearance of a shake-up satellite peak at 946 eV validates the presence of Cu^{2+}.[40] This satellite peak can be caused by the charge transfer between ligands (O^{2-} from CuO) and unfulfilled valence levels (d^9) of the Cu^{2+} ion.[40]

Fig. 3 compares the XPS spectra of NCM/MgO and NCM samples. A specific Mg 2p peak at 49.21 eV is present in the spectrum of the coated material. The binding energy of Mg matches with that of MgO, thereby suggesting +2 oxidation state for Mg.[33] Moreover, peaks of other elements do not show any observable binding energy shifts after MgO coating. Thus, it can be concluded that MgO is uniformly coated on the surface without altering the chemical environment of the native compound. The appearance of sharp O 1s peak after MgO coating could be due to surface-adsorbed water molecules with OH^- or O bonded to their surface.[41]

Electrochemical performance of all the samples was examined using coin-type cells with Na metal as the counter and reference electrode. It is notable that the electrochemical activity of layered oxides was greatly influenced by cut-off voltages;[42] hence, we initially chose a lower testing window of 2.2–4.25 V *vs.* Na. Fig. 4a and b compare the initial voltage–capacity profiles and long-term cycling stability of NM and NCM in a voltage range of 2.2–4.25 V *vs.* Na at a rate of 0.25C (34 mA g^{-1}). The NM electrode shows an initial discharge capacity of 115 mA h g^{-1}, with three distinct voltage plateaus at 3.35, 3.71, and 4.23 V *vs.* Na. The capacity in the low-voltage range of 2.1–2.4 V *vs.* Na is ascribed to Mn^{3+}/Mn^{4+} redox reaction, while Ni^{2+}/Ni^{4+} redox reaction contributes at higher potentials.[19] The remaining voltage plateau below 4.0 V *vs.* Na was due to the presence of Na^+/vacancy ordering and the stalking faults arising from

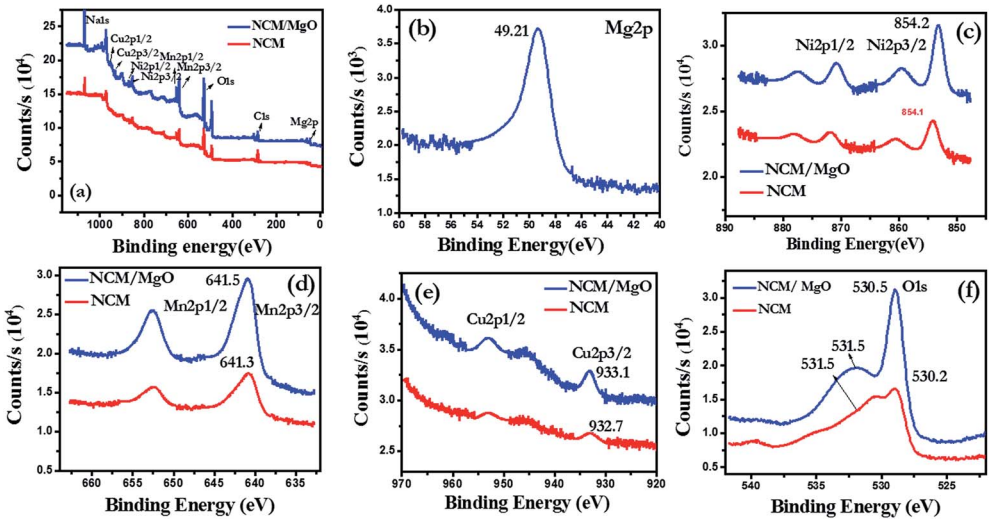

Fig. 3 (a) Survey spectrum of NCM and NCM/MgO, core level spectra of (b) Mg 2p, (c) Ni 2p, (d) Mn 2p, (e) Cu 2p, and (f) O 1s.

transition metal layer gliding.[19] The long plateau appearing at 4.2 V *vs.* Na for NM is due to the mostly reversible P2–O2 phase transition *via* an intermediate OP4 phase, as reported by Lee *et al.*[19,39] This phenomenon is a major practical issue for realizing high-rate cathode materials for SIB and can be easily explained by the structural arrangements of atoms. In P2 and O2 structures, Na-ions were located at prismatic and octahedral sites with AABB and ABCB stacking sequences, respectively.[43] Hence, O2 structure could easily be formed by a simple gliding of oxygen layers without breaking the O–TM bonds. The driving force for this phase transition is the higher coulombic repulsion of the adjacent oxygen layers when more Na ions are removed at higher potentials.[19] *In situ* and *ex situ* XRD studies have been used by several research groups to confirm the phase change occurring in this voltage range.[18,42]

NCM was found to deliver a discharge capacity of 110 mA h g^{-1} when cycled at 0.25C in voltage range of 2.2–4.25 V *vs.* Na. It was evident that a small amount of Cu in the lattice was sufficient to smoothen the plateau at higher voltages at the expense of a small capacity due to the electrochemically inactive nature of the Cu ion. The average voltage was also enhanced, leading to higher energy density. NM was cycled 100 times in voltage window of 2.2–4.25 V *vs.* Na, and the plot is shown in Fig. 4b. It can be observed that all samples could reversibly intercalate and de-intercalate Na ions within the layered structure for a long time. The long-term cycling performance of NM can be best described by its higher initial discharge capacity along with a high capacity fade until the tenth cycle, followed by more stable long-term cycling. The capacity retention after 25 cycles was 77.93%, with the discharge capacity equaling 94 mA h g^{-1}. The capacity was found to decrease gradually until the 100th cycle, with the final capacity retention equaling 70.75% and the final capacity being 81 mA h g^{-1}. The coulombic efficiency in the final cycles reached 97.87%. The capacity fade at initial voltages can be attributed to several phenomena like (i) electrolyte decomposition, which resulted in the formation of a solid–electrolyte interface (SEI) layer,[44] (ii) Jahn–Teller distortion resulting in Mn^{2+} dissolution into the electrolyte,[45] (iii) severe internal stress with a significant volume change, resulting from the accommodation of larger sized Na ions,[46] and (iv) insertion of solvated ions into the metal oxide layers.[47] Copper was utilized as an inactive metal ion for crystal structure stabilization and disruption of Na^+/vacancy ordering. The initial discharge capacity of Cu-substituted NCM was 111 mA h g^{-1}, which was lower than that of NM (Fig. 4a). This lower value can be attributed to the presence of electrochemically inactive Cu species. However, substitution by copper smoothens the voltage plateau above 3.5 V *vs.* Na, thereby reducing the phase gliding due to deep extraction of Na at higher voltages. The long-term cycling performance of NCM was compared to that of NM to determine the effect of Cu doping. For NCM, the initial capacity fade up to the 25th cycle was significantly reduced and the capacity retention was equal to 90.27% after 50 cycles. After 50 cycles, the observed discharge capacity equaled 100 mA h g^{-1}, which was 10 mA h g^{-1} higher than that of the pristine material. The discharge capacity dropped to 92 mA h g^{-1} after 100 cycles,

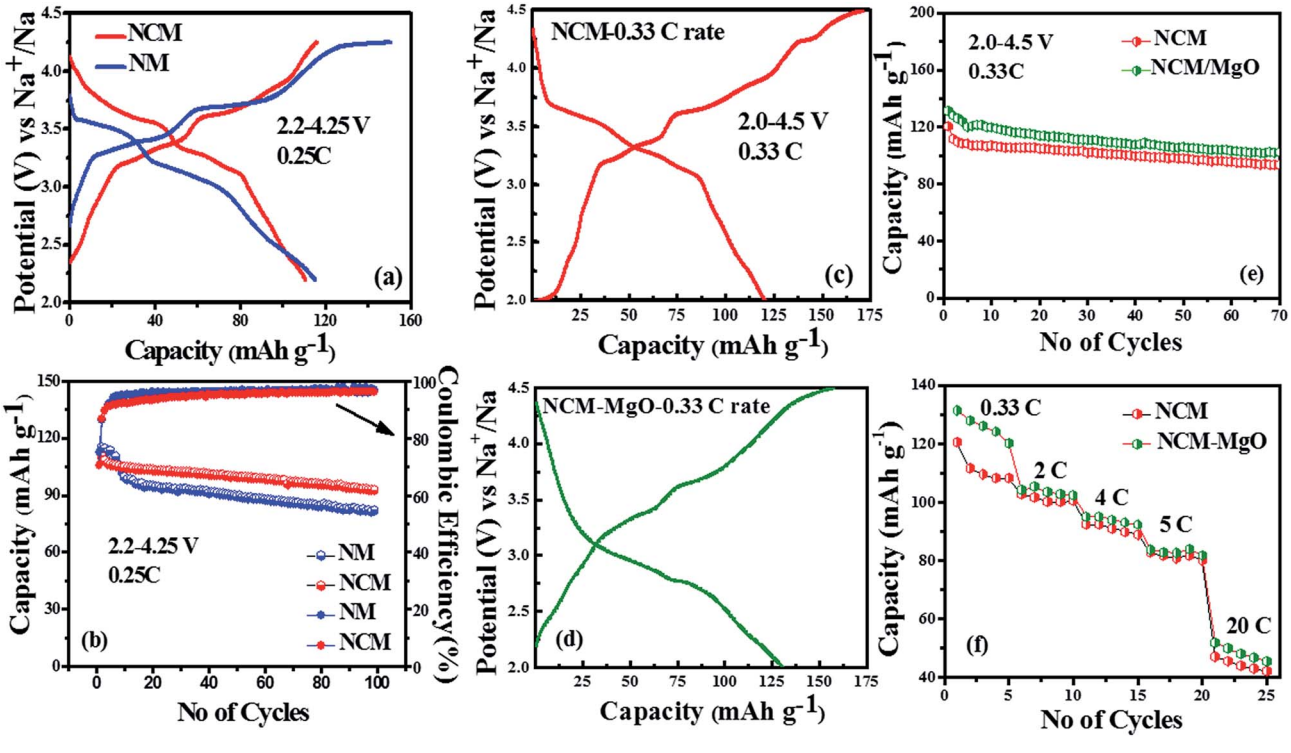

Fig. 4 (a) Initial galvanostatic charge/discharge profile and (b) cycling performance of NM and NCM at 0.25C in a voltage range of 2.2–4.25 V *vs.* Na. (c and d) Initial galvanostatic charge/discharge cycles of NCM and NCM/MgO, (e) cycling performance of NCM and NCM/MgO, and (f) rate performance of NCM and NCM/MgO at 0.33C in a voltage range of 2.0–4.5 V *vs.* Na.

resulting in a capacity retention of 83.63%. When NCM was further analyzed in an extended voltage window of 2.0–4.5 V at a rate of 0.33C (45 mA g^{-1}), an initial discharge capacity of 120 mA h g^{-1} was obtained due to increased participation of Na ions. The effect of Cu substitution was highlighted by the smooth and enhanced voltage plateau of NCM.

It can be noted that phase transitions alone cannot be responsible for the capacity fade at high cut-off voltages, indicating the existence of other driving forces mentioned above. Hence, surface coating was a good strategy to prevent direct contact of the cathode material with electrolyte and improve its interfacial properties. Thus, we coated the surface of NCM with a thin layer of MgO by melt impregnation and studied its electrochemical performance in a high-voltage range of 2.0–4.5 V *vs.* Na. Surprisingly, the initial discharge capacity was significantly increased to 131 mA h g^{-1}. Moreover, the smooth voltage curve of MgO-coated NCM (Fig. 4d) indicated suppression of the partially irreversible P2–O2 phase transition at 4.2 V *vs.* Na, which was very important for P2–Na–Ni–Mn–O based cathodes at higher cut-off voltages. When long-term cycling performance was analyzed at the same input conditions (Fig. 4e), a significantly smaller initial capacity fade was observed with an enhanced capacity retention of 96.45% even after 70 cycles. Liu *et al.*[48] studied the capacity degradation mechanism of $Na_{2/3}Ni_{1/3}Mn_{2/3}O_2$ using Al_2O_3 coating and retained only 88.4% after 50 cycles. However, this study did not address the P2–O2 phase transition of cathode that occurs above 4.2 V. When bare NCM was charged to high voltage, more Na ions were extracted from the lattice, initiating the exfoliation of the layered structure[48] and resulted in a capacity fade over prolonged cycles. To understand Cu doping and MgO coating in the layered structure, differential capacity plots were drawn from the charge/discharge curves (Fig. S6†). In Fig. S6a and b,† multiple redox peaks were found in the voltage range of 2.20–4.25 V, corresponding to the voltage plateaus in the charge–discharge profiles. The peaks above 3.0 V resulted from the redox reaction of Ni^{2+}/Ni^{4+} couples, whereas the peaks below 3.0 V arose due to the contribution of Mn^{3+}/Mn^{4+} couple. The separations between anodic and cathodic peaks were significantly reduced for Cu-doped samples, thereby proving the improved stability of the cathode. When the voltage windows were further expanded, a clear peak was observed at around 4.2 V in the charge curve of NCM (Fig. S6c†). In case of MgO coated NCM, the peaks became broader with less intensity, indicating smooth structural transition over the entire voltage range and a complete suppression of the peak at 4.2 V (Fig.-S6d†). To ascertain the role of MgO coating, we studied 2 wt% of MgO coated over NM at high voltage window. Although, a small reduction in the initial capacity was observed for MgO coated NM, it rendered better stability with high capacity retention characteristics after 15 cycles (Fig. S7†). Moreover, to understand the influence of MgO coating, we coated NCM with 1, 2 and 5 wt% of MgO and cycled at different current rates. Among these, 2 wt% MgO was found to be the optimum concentration to yield a high performance cathode with better rate capability (Fig. S8†). From the above results, MgO coating was found to have a major role in improving the electrochemical performance of high voltage cathodes. Further analysis of structure using *in situ* monitoring techniques would provide a deeper understanding of the mechanism behind MgO coating.

Rate capability is an important factor for large-scale applications of SIB. Hence, the rate capability of the above mentioned materials was analyzed in a voltage range of 2.0–4.5 V at current densities from 0.33 to 20C (1C = 136 mA h g^{-1}), as depicted in Fig. 4f. The NCM displayed specific capacities of 120, 103, 92, 83, and 47 mA h g^{-1} at current densities of 0.33, 2, 4, 5, and 20C, respectively, whereas NCM/MgO exhibited enhanced specific capacities of 131, 104, 95, 84, and 52 mA h g^{-1}, respectively. If we define the discharge capacity of 131 mA h g^{-1} at 0.33C as 100%, the cell could be operated at high rates, maintaining normalized capacity values of 79%, 72%, 63%, and 39% at current rates of 2 (272 mA g^{-1}), 4 (544 mA g^{-1}), 5 (680 mA g^{-1}) and 20C (2720 mA g^{-1}), corresponding to initial discharge cycle at each rate. The cathode capacity decreased with increasing current density due to improper utilization of active materials at high input currents. Even at high current rates of 5 and 20C, the coated material exhibited capacities of 84 and 51 mA h g^{-1}, respectively. The transport of electrons from the cathode to current collector was the critical step at high current rates, promoted by modification of the surface with MgO. In addition, MgO coating decreased the activation energy for charge transfer reaction at electrode/electrolyte interface.[49] Based on the above results, MgO coating provided a mechanical support to the cathode at high operation voltages. Even the high-capacity $Na_{0.5}Ni_{0.23}Fe_{0.13}Mn_{0.63}O_2$ cathode reported by Hasa *et al.*[50] could only deliver a capacity of 60 mA h g^{-1} at a rate of 5C. Recently, Li *et al.*[51] have reported $Na_{0.67}Mn_{0.8}Ni_{0.1}Mg_{0.1}O_2$ as a high-rate NIB cathode material using a novel design strategy. This material delivered a specific capacity of only 66 mA h g^{-1} at 5C. Numerous reports on P2-type layered cathode materials along with their high-rate capacities are listed in Table 1. Apparently, our results displayed one of the best set of values compared to other reported values for Na–Ni–Mn–O-based cathodes with metal-substituted derivatives; for example, Komaba group[52] reported $Na_{2/3}Ni_{1/3}Mn_{2/3-x}Ti_xO_2$ as a high-energy NIB cathode that can deliver *ca.* 90 mA h g^{-1} at

Table 1 Comparison of previously reported studies with our study

Sample	Current rate/C	Capacity/ mA h g^{-1}	Voltage/V *vs.* Na	Reference
$Na_{0.45}Ni_{0.22}Co_{0.11}Mn_{0.66}O_2$	5/2	76/91	2.1–4.3	53
$Na_{0.5}Ni_{0.23}Fe_{0.13}Mn_{0.63}O_2$	5	60	1.5–4.6	50
$Na_{0.45}Ni_{0.22}Co_{0.11}Mn_{0.66}O_2$	5/2	75/127	2.0–4.2	54
P2-$Na_{0.66}Mn_{0.8}Fe_{0.1}Ti_{0.1}O_2$	5/2	~60/67	2.0–4.0	55
P2-$Na_{0.7}Mn_{0.60}Ni_{0.30}Co_{0.10}O_2$	1	>75	1.7–4.0	56
P2-$Na_xFe_{1/2}Mn_{1/2}O_2$	4	>60	1.5–4.2	57
P2-$Na_{2/3}Ni_{1/3}Mn_{2/3-x}Ti_xO_2$	2	>90	2.5–4.5	52
$Na_{0.67}Ni_{0.25}Mg_{0.1}Mn_{0.65}O_2$	1	70	2.0–4.2	23
$Na_{0.80}[Li_{0.12}Ni_{0.22}Mn_{0.66}]O_2$	5	71	2.0–4.4	22
$Na_{0.67}Mn_{0.80}Ni_{0.1}Mg_{0.1}O_2$	5	66	1.5–4.2	51
$Na_{0.5}Ni_{0.26}Cu_{0.07}Mn_{0.67}O_2$	5/2	**83/104**	2.0–4.5	**Present study**

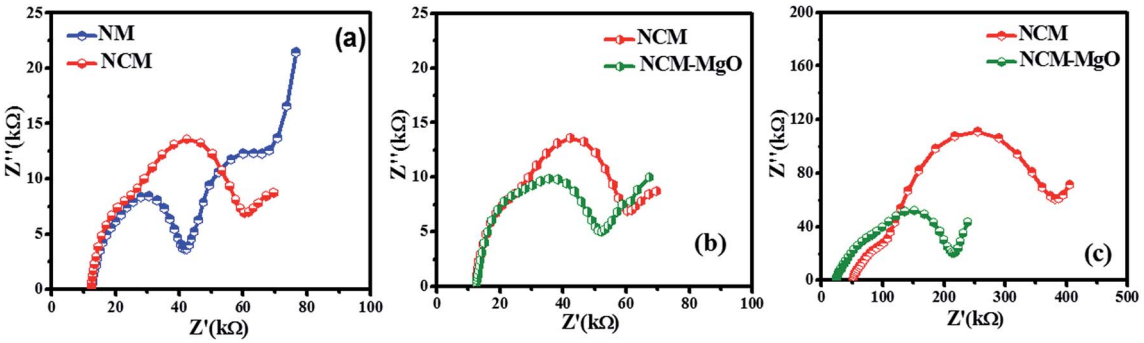

Fig. 5 Nyquist plots of (a) NM and NCM before cycling, (b) NCM and NCM/MgO before cycling in voltage range of 2.0–4.5 V *vs.* Na and (c) NCM and NCM/MgO after cycling in voltage range of 2.0–4.5 V *vs.* Na.

a rate of 2C. As evidenced by structural analysis, the enlarged *c*-axis and increased volume upon Cu-ion substitution facilitate wider Na-ion diffusion paths even at high current rates. Hence, this high rate performance can meet the demands of large-scale applications.

To further evaluate the kinetic properties, EIS was used as a major tool. Fig. 5a shows the Nyquist plots of NM and NCM before cycling. The NM plot exhibits three regions with a depressed semicircle in the high-frequency region, followed by a semicircle in the high to medium frequency, and a quasi-straight line in the low frequency region, corresponding to surface resistance (SEI layer), charge transfer resistance (R_{ct}), and Warburg impedance, respectively.[17] Clearly, the charge transfer resistance was very much reduced for Cu-doped sample, compared to that of the pristine material. This was due to the rapid charge transfer at the electrode/electrolyte interface and enhanced reaction kinetics of the electrode material. Moreover, the absence of a proper semicircle in the high-frequency region of the doped material denoted negligible role of resistance caused by diffusion of Na^+ ions in SEI layer. The functional introduction of Cu ions into the crystal structure plays a critical role in improving the Na-ion diffusion of NCM sample by altering the local structure of cathode material. These results agree well with the excellent cycling stability exhibited by the doped material in the limited cut-off voltage range.

To clearly understand the influence of MgO coating on the cycling performance at high voltages, Nyquist plots of NCM and NCM/MgO samples were recorded before and after 70 cycles (Fig. 5b). Initially, the charge transfer resistance of MgO-coated sample was very much reduced compared to that of the native compound, with the latter exhibiting feasible Na-ion diffusion and electronic conduction at high current rates, as reported by Karthikeyan *et al.*[31] Fig. 5c shows Nyquist plots of NCM and NCM/MgO after 70 cycles. The appearance of a single semicircle in high-frequency region for MgO-coated sample indicates its reduced charge transfer resistance and the negligible role of interfacial resistance caused by SEI layer formation, which very well accounts for the long-term cycling performance of this sample. The MgO encapsulation over NCM certainly hinders unwanted side reaction with electrolyte and subsequently prevents the formation of by-products in the form of SEI layer over the active material surface. This eventually facilitates the smooth transfer of ions and electrons over prolonged cycles.[33] Hence, these observations show the functional role of MgO coating in improving the electrochemical performance of layered oxides at high operating voltages. This study provides a new way of designing high-rate cathode materials for future SIB applications.

4. Conclusion

In summary, MgO-coated P2-type $Na_{0.5}Ni_{0.26}Cu_{0.07}Mn_{0.67}O_2$ (NCM) was developed as a high-rate cathode for SIB applications. The presence of Cu in the lattice effectively minimized Na^+/vacancy ordering and improved structural stability, leading to capacity retention of 83% after 100 cycles. MgO-modified NCM sample showed an initial discharge capacity of 131 mA h g^{-1} with an improved voltage profile in a voltage range of 2.0–4.5 V. Finally, all the above results confirm that MgO coating (i) suppressed P2–O2 phase transformation at high voltages, (ii) stabilized the SEI layer formed during initial cycles, and (iii) prevented metal-ion dissolution, resulting in reduced phase transition and higher rate performance of the NCM cathode. Hence, substitution with a suitable amount of inactive metal ions and modifying the cathode surface with a proper metal oxide coating play multiple roles in improving the high-voltage electrochemical performance of P2-type layered oxides, providing new insights into designing high-rate cathode materials for SIBs.

Acknowledgements

This study was supported by the National Research Foundation of Korea (NRF) grant funded by the Korea government (Ministry of Science, ICT & Future Planning) (No. 2016R1A4A1012224).

References

1 N. Yabuuchi, K. Kubota, M. Dahbi and S. Komaba, *Chem. Rev.*, 2014, **114**, 11636–11682.
2 D. Buchholz, L. G. Chagas, M. Winter and S. Passerini, *Electrochim. Acta*, 2013, **110**, 208–213.
3 X. Xiang, K. Zhang and J. Chen, *Adv. Mater.*, 2015, **27**, 5343–5364.
4 L. P. Wang, L. Yu, X. Wang, M. Srinivasan and Z. J. Xu, *J. Mater. Chem. A*, 2015, **3**, 9353–9378.

5 D. Yuan, X. Hu, J. Qian, F. Pei, F. Wu, R. Mao, X. Ai, H. Yang and Y. Cao, *Electrochim. Acta*, 2014, **116**, 300–305.
6 S. M. Oh, S. T. Myung, J. Hassoun, B. Scrosati and Y. K. Sun, *Electrochem. Commun.*, 2012, **22**, 149–152.
7 W. Deng, X. Liang, X. Wu, Z. Qian, Y. Cao, X. Ai, J. Feng and H. Yang, *Sci. Rep.*, 2013, **3**, 1–6.
8 Y. You, X. L. Wu, Y. X. Yin and Y.-G. Guo, *Energy Environ. Sci.*, 2014, **7**, 1643.
9 M. H. Han, E. Gonzalo, G. Singh and T. A. Rojo, *Energy Environ. Sci.*, 2014, **8**, 81–102.
10 C. Delmas, C. Fouassier and P. Hagenmuller, *Physica B+C*, 1980, **99**, 81–85.
11 S. C. Han, H. Lim, J. Jeong, D. Ahn, W. B. Park, K. S. Sohn and M. Pyo, *J. Power Sources.*, 2015, **277**, 9–16.
12 P. Vassilaras, X. Ma, H. Chen and G. Ceder, *J. Electrochem. Soc.*, 2013, **160**, A1207.
13 J. Billaud, G. Singh, A. R. Armstrong, E. Ganzalo, V. Roddatis, M. Armand, T. Rojo and P. G. Bruce, *Energy Environ. Sci.*, 2014, **7**, 1387.
14 N. Yabuuchi, H. Yoshida and S. Komaba, *Electrochemistry*, 2012, **80**, 716–719.
15 D. Yuan, W. He, F. Pei, F. Wu, Y. Wu, J. Qian, Y. Cao, X. Ai and H. Yang, *J. Mater. Chem. A*, 2013, **1**, 3895.
16 J. L. Yue, W. W. Yin, M. H. Cao, S. Zulipiya, Y. N. Zhou and Z. W. Fu, *Chem. Commun.*, 2015, **51**, 1–4.
17 X. Wu, J. Guo, D. Wang, G. Zhong, M. J. Mcdonald and Y. Yang, *J. Power Sources*, 2015, **281**, 18–26.
18 Z. Lu and J. R. Dahn, *J. Electrochem. Soc.*, 2001, **148**, A1225.
19 D. H. Lee, J. Xu and Y. S. Meng, *Phys. Chem. Chem. Phys.*, 2013, **15**, 3304.
20 W. Zhao, H. Kirie, A. Tanaka, M. Unno, S. Yamamoto and H. Noguchi, *Mater. Lett.*, 2014, **135**, 131–134.
21 H. Yoshida, N. Yabuuchi, K. Kubota, I. Ikeuchi, A. Garsuch, M. S. Dobrick and S. Komaba, *Chem. Commun.*, 2014, **50**, 3677.
22 J. Xu, D. H. Lee, R. J. Clement, X. Yu, M. Leskes, A. J. Pell, G. Pintacuda, X. Q. Yang, C. P. Grey and Y. S. Meng, *Chem. Mater.*, 2014, **26**, 1260–1269.
23 K. Hemalatha, M. Jayakumar, P. Bera and A. S. Prakash, *J. Mater. Chem.*, 2015, **3**, 20908–20912.
24 C. Nithya, R. Thirunakaran, A. Sivashanmugam and S. Gopukumar, *J. Power Sources*, 2011, **196**, 6788.
25 K. R. Chemelewski and A. Manthiram, *J. Phys. Chem. C*, 2013, **117**, 12465.
26 M.-C. Yang, B. Xu, J.-H. Cheng, C.-J. Pan, B.-J. Hwang and Y. S. Meng, *Chem. Mater.*, 2011, **23**, 2832.
27 S. Y. Xu, X. Y. Wu, Y. M. Li, Y. S. Hu and L. Q. Chen, *Chin. Phys. B*, 2014, **23**, 118202.
28 L. Q. Mu, Y. S. Hu and L. Q. Chen, *Chin. Phys. B*, 2015, **24**, 038202.
29 Y. Ono, Y. Yui, M. Hayashi, K. Asakura, H. Kitabayashi and K. I. Takahashi, *ECS Trans.*, 2014, **58**, 33–39.
30 M. Doeff, T. Richardson, J. Hollingsworth, C. W. Yuan and M. Gonzales, *J. Power Sources*, 2002, **112**, 294–297.
31 K. Karthikeyan, J. Liu, A. Lushington, R. Li and X. Sun, *ChemSusChem*, 2015, **8**, 2537–2543.
32 P. Yan, J. Zheng, X. Zhang, R. Xu, K. Amine, J. Xiao, J. G. Zhang and C. M. Wang, *Chem. Mater.*, 2016, **28**, 857–863.
33 S. J. Shi, J. P. Tu, Y. Y. Tang, X. Y. Liu, Y. Q. Zhang, X. L. Wang and C. D. Gu, *Electrochim. Acta*, 2013, **88**, 671–679.
34 J. Z. Kong, S. S. Wang, G. A. Tai, L. Zhu, L. G. Wang, H. F. Zhai, D. Wu, A. D. Li and H. Li, *J. Alloys Compd.*, 2016, **657**, 593–600.
35 F. Wu, Z. Wang, Y. Su, N. Yan, L. Bao and S. Chen, *J. Power Sources.*, 2014, **247**, 20–25.
36 S. J. Kim, M. C. Kim, D. H. Kwak, D. M. Kim, G. H. Lee, H. S. Choe and K. W. Park, *J. Power Sources*, 2016, **304**, 119–127.
37 J. H. Shim, S. Lee and S. S. Park, *Chem. Mater.*, 2014, **26**, 2537–2543.
38 W. Zhao, A. Tanaka, K. Momosaki, S. Yamamoto, F. Zhang, Q. Guo and H. Noguchi, *Electrochim. Acta*, 2015, **170**, 171–181.
39 L. G. Chagas, D. Buchholz, C. Vaalma, L. Wu and S. Passerini, *J. Mater. Chem. A*, 2014, **2**, 20263–20270.
40 J. Hernandez, P. Wrschka and G. S. Oehrlein, *J. Electrochem. Soc.*, 2001, **148**, G389.
41 S. H. Yuna, K. S. Park and Y. J. Park, *J. Power Sources*, 2010, **195**, 6108–6115.
42 H. Wang, B. Yang, X. Z. Liao, J. Xu, D. Yang, Y. S. He and Z. F. Ma, *Electrochim. Acta*, 2013, **113**, 200–204.
43 X. Qi, Y. Wang, L. Jiang, L. Mu, C. Zhao, L. Liu, Y. S. Hu, L. Chen and X. Huang, *Part. Part. Syst. Charact.*, 2015, 1–7.
44 K. Karthikeyan, S. Amaresh, G. W. Lee, V. Aravindan, H. Kim, K. S. Kang, W. S. Kim and Y. S. Lee, *Electrochim. Acta*, 2012, **68**, 246–253.
45 Y. Wen, B. Wang, G. Zeng, K. Nogita, D. Ye and L. Wang, *Chem.–Asian J.*, 2015, **10**, 661–666.
46 Z. Jian, W. Han, X. Lu, H. Yang, Y. S. Hu, J. Zhou, Z. Zhou, J. Li, W. Chen, D. Chen and L. Chen, *Adv. Energy Mater.*, 2013, **3**, 156–160.
47 S. Komaba, N. Yabuuchi, T. Nakayama, A. Ogata, T. Ishikawa and L. Nakai, *Inorg. Chem.*, 2012, **51**, 6211–6220.
48 Y. Liu, X. Fang, A. Zhang, C. Shen, Q. Liu, H. A. Enaya and C. Zhou, *Nano Energy*, 2016, **27**, 27–34.
49 H. Zhao, L. Gao, W. Qiu and X. Zhang, *J. Power Sources*, 2004, **132**, 195–200.
50 I. Hasa, D. Buchholz, S. Passerini, B. Scrosati and J. Hassoun, *Adv. Energy Mater.*, 2014, **4**, 0–6.
51 Z. Li, R. Gao, J. Zhang, X. Zhang, Z. Hu and X. Liu, *J. Mater. Chem. A*, 2016, **4**, 3453–3461.
52 H. Yoshida, N. Yabuuchi, K. Kubota, I. Ikeuchi, A. Garsuch, M. S. Dobrick and S. Komaba, *Chem. Commun.*, 2014, **50**, 3677–3680.
53 D. Buchholz, A. Moretti, R. Kloepsch, S. Nowak, V. Siozios, M. Winter and S. Passerini, *Chem. Mater.*, 2013, **25**, 142–148.
54 D. Buchholz, L. G. Chagas, M. Winter and S. Passerini, *Electrochim. Acta*, 2013, **110**, 208–213.
55 M. H. Han, E. Gonzalo, N. Sharma, J. M. L. D. Amo, M. Armand, M. Avdeev, J. J. S. Garitaonandia and T. Rojo, *Chem. Mater.*, 2016, **28**, 106–116.
56 J. Yoshida, E. Guerin, M. Arnault, C. Constantin, B. M. D. Boisse, D. Carlier, M. Guignard and C. Delmas, *J. Electrochem. Soc.*, 2014, **161**(14), A1987–A1991.
57 N. Yabuuchi, M. Kajiyama, J. Iwatate, H. Nishikawa, S. Hitomi, R. Yokuyama, R. Usui, Y. Yamada and S. Komaba, *Nat. Mater.*, 2012, **11**, 512–517.